Connecting genetic incompatibilities with natural selection on additive genetic variation during adaptive radiation

Greg M. Walter[1*], *J. David Aguirre*[2], *Melanie J Wilkinson*[1], *Thomas J. Richards*[3], *Mark W. Blows*[1] *and Daniel Ortiz-Barrientos*[1]

[1]University of Queensland, School of Biological Sciences, St. Lucia QLD 4072, Australia

[2]Massey University, School of Natural and Computational Sciences, Auckland 0745, New Zealand

[3]Swedish University of Agricultural Science, Department of plant Biology, Uppsala, 75007, Sweden

* Corresponding Author: Greg M. Walter

Email: g.walter@bristol.ac.uk

Address: School of Biological Sciences, Life Sciences Building

University of Bristol, Bristol, UK BS8 1TQ

Keywords: natural selection, trade-offs, additive genetic variance, selection gradient, response to selection, adaptive divergence, adaptive radiation, genetic incompatibilities, reproductive isolation, macroevolution

Abstract

Evolutionary biologists have long sought to identify the links between micro and macroevolution to better understand how biodiversity is created. Despite this pursuit, it remains a challenge to understand how allele frequency changes correlate with the evolution of morphological diversity, and the build-up of reproductive isolation amongst taxa. To connect mechanisms of microevolution with patterns of diversification, we tested the adaptive importance of alleles underlying genetic incompatibilities, and the consequences for predicting evolutionary trajectories of multiple ecotypes of an Australian wildflower. Using a quantitative genetics crossing design, we produced an F4 generation Advanced Recombinant Form (ARF) between four contrasting ecotypes, which we phenotyped in the glasshouse (N=770) and transplanted into the four natural habitats (N=14,265 seeds), alongside the parental ecotypes. F2 hybrid breakdown was associated with the loss of extreme phenotypes and habitat-specific genetic variation in field performance. Genetic trade-offs existed among habitats, but only in axes describing smaller amounts of genetic variance for fitness. Habitats that showed stronger patterns of adaptive divergence for native versus foreign ecotypes, also showed lower genetic variance in fitness of the ARF. Integrating data from the field and glasshouse predicted patterns of selection on morphological traits in a similar direction to the parental ecotypes. Overall, our results provide strong empirical evidence linking ecotype specific alleles with phenotypic divergence, fitness trade-offs, rapid adaptation and the accumulation of genetic incompatibilities among recently derived ecotypes. Our data connects microevolutionary change with macroevolution through adaptive radiation, where selection for environment specific alleles creates rapid adaptive divergence leading to speciation.

Introduction

Historically, evolutionary biologists have long discussed the link between adaptation and speciation to understand how natural selection can reconcile microevolutionary genetic changes with macroevolutionary species diversification. We know that natural selection acts largely upon the additive effects of genes (Hill et al. 2008), but we also widely accept that species form when interactions among genes create intrinsic reproductive isolation between diverging lineages (Dobzhansky 1937; Muller 1942). Therefore, adaptation occurs when natural selection increases the frequency of beneficial alleles, but the role of these same alleles in creating intrinsic reproductive isolation remains unresolved. This gap in our understanding of evolution is largely due to the difficulty of estimating natural selection in the wild (Pujol et al. 2018), and connecting it to the accumulation of intrinsic reproductive isolation (Baack et al. 2015). A more detailed understanding of natural selection can identify whether alleles underlying adaptation are also those contributing to reproductive isolation, and how this leads to adaptive radiation.

Alleles can confer an adaptive advantage in one environment, but with deleterious effects in other environments, leading to fitness tradeoffs (Anderson et al. 2011; Anderson et al. 2013). If environment specific alleles evolve in the absence of gene flow, they will be novel in relation to genotypes from alternative environments and could fail when tested in alternative genetic backgrounds, creating reproductive isolation (Coyne and Orr 2004). Under this scenario, environment specific alleles can lead to the evolution of Bateson-Dobzhansky-Muller genetic incompatibilities when incompatible with alternative genetic backgrounds (Dobzhansky 1937; Muller 1942), meaning alleles underlying adaptive traits in one ecotype can lead to hybrid breakdown when they are introgressed into an alternative ecotype (Kondrashov 2003; Navarro and Barton 2003). Using artificial hybridization to simulate gene flow among divergent ecotypes, we can assess the consequences for phenotypic and genetic variation before and after genetic incompatibilities arise. If alleles underlying adaptation to contrasting environments concomitantly create fitness trade-offs and reproductive isolation, we can use changes in environment specific allele frequencies to connect micro and macroevolution.

Natural selection is unlikely to affect single traits in isolation, favoring beneficial combinations of traits and the evolution of multivariate phenotypes (Lande 1979; Cheverud 1982). Adaptation will be constrained when traits share genetic variance and genetic architecture, rather than natural selection, determines evolutionary trajectories (Lande and Arnold 1983; Arnold 1992; Schluter 1996). In this way, adaptive alleles will likely increase in frequency, but only if selection on genetically correlated traits allow it. Genetic correlations are expected to remain stable, at least in the short term, which would make rapid adaptive divergence leading to adaptive radiation difficult (Walsh and Blows 2009). However, recent studies have shown that matrices that capture the genetic relationship among traits (G-matrices) can potentially evolve rapidly (Doroszuk et al. 2008; Eroukhmanoff and Svensson 2011; Walter et al. 2018a), questioning the role of constraints in adaptive radiation. If genetic correlations can evolve in response to natural selection, then environment specific allele frequency changes can overcome genetic constraints to promote rapid adaptive divergence, and the path to adaptive radiation will be more straightforward. However, the consequences of this evolutionary release might impact the ability of populations to interbreed, incidentally leading to the evolution of intrinsic reproductive isolation.

We explore the evolutionary connection between adaptation and speciation using the adaptive radiation of an Australian native wildflower, *Senecio pinnatifolius*. We focus on four ecotypes within this species complex including two coastal types found on sandy dunes (Dune ecotype, *Senecio pinnatifolius* var. *pinnatifolius*) and rocky headlands (Headland ecotype, *S. pinnatifolius* var. *maritimus*), and two inland ecotypes that occur in moist sub-tropical rainforest (Tableland ecotype, *S. pinnatifolius* var. *serratus*) and dry sclerophyll woodland (Woodland ecotype, *S. pinnatifolius* var. *dissectifolius*) (Ali 1969; Radford et al. 2004). Previous work has shown that these ecotypes arose as a result of adaptation to divergent natural selection (Melo et al. 2014; Walter et al. 2016), resulting in habitat specific plant morphologies, fitness trade-offs and immigrant inviability among contrasting habitats (Melo et al. 2014; Richards and Ortiz-Barrientos 2016; Richards et al. 2016; Walter et al. 2016; Walter et al. 2018a; Walter et al. 2018b). Artificial hybridization among ecotypes produced vigorous F1 offspring, with hybrid breakdown observed at the F2 generation as a strong reduction in reproductive capacity, suggesting incompatible alleles have arisen among ecotypes. Fitness recovery in the subsequent generation suggested genetic

incompatibilities arose as a breakup of coadapted gene complexes (Walter et al. 2016). Combined with evidence of a recent origin (Roda et al. 2013a), patterns of morphological and reproductive divergence suggest these ecotypes have recently undergone adaptive radiation.

Here, we employ a combination of glasshouse and field experiments to explore the implications of artificial hybridization during adaptive radiation. Using a quantitative genetic crossing design among the four ecotypes, we created an F4 generation advanced recombinant form (ARF). Alongside the parental ecotypes, we phenotyped the ARF in the glasshouse and performed a large-scale field transplant across the four natural habitats. If ecotype specific alleles connect adaptation and speciation during adaptive radiation, we hypothesized that following F2 hybrid breakdown we would observe: 1) Reductions in phenotypic variance compared to parental ecotypes, 2) Low genetic variance for fitness in habitats associated with stronger adaptive divergence in parental ecotypes, 3) Reduced genetic trade-offs among habitats compared to parental ecotypes, and 3) Habitat specific selection gradients that align with the direction of phenotypic divergence in the parental ecotypes. Testing these predictions, we demonstrate that adaptive radiation was produced by ecotype specific alleles that created phenotypic divergence, adaptive genetic variance, genetic incompatibilities and reduced genetic constraints to adaptation.

Methods

Crossing design

To create the ARF we first sampled seeds from one natural population from each of the four ecotypes, which we germinated and grew at the University of Queensland glasshouses. We sampled seeds for the Dune and Headland ecotypes at Lennox Head, NSW (*-28.783005, 153.594018* and *-28.813117, 153.605319*, respectively), from the Tableland ecotype at O'Reilley's Rainforest Retreat, Qld (*-28.230508, 153.135078*) and the Woodland ecotype at Upper Brookfield, Qld (*-27.479946, 152.824709*). At each location, we collected seeds from 24-49 plants separated from each other by at least 10 m to minimize the likelihood of sampling close relatives. Two seeds from each individual sampled were germinated and grown in the University of Queensland glasshouses, which then formed the base population for our crossing design, outlined below. To grow plants, we first scarified each seed and

placed them in glass petri dishes containing moist filter paper. After leaving them in the dark for two days we transferred the germinated seeds to a 25°C constant temperature growth room with 12h:12h light:dark photoperiod. After one week, we transferred the seedlings to the glasshouse and transplanted them into 85mm pots containing a mixture of 70% pine bark and 30% coco peat with slow release osmocote fertilizer and 830g/m^3 of Suscon Maxi insecticide. We conducted controlled crosses on mature plants by rubbing two mature flower heads together, labeling the flower heads and collecting the seeds as they emerged.

We created the ARF ensuring each ecotype contributed equally and ensuring that at each generation (see Figure 1C), all full-sibling families (hereafter, 'families') contributed equally to the next generation. First, we grew plants for the base population from seeds sampled from the natural populations and performed crosses among the ecotypes (n = 41-60 individuals/ecotype) to create all combinations of F1 hybrids (n = 12 crossing combinations; n = 20-25 families/cross type). We then mated among all combinations of crosses in the F1 generation such that all F2 families (n = 24 crossing combinations; n = 17-22 families /cross type) possessed a grandparent from each of the original parental ecotypes (e.g., $F1_{Dune,Headland} \times F1_{Tableland,Woodland}$). Given strong reductions in intrinsic fitness was observed in a previous Dune x Headland F2 hybrid (Walter et al. 2016), we maximized the number of F1 crosses to produce 458 F2 families in total. We grew one individual from each family. Reductions in fitness were observed as F2 hybrid sterility (42% of F2 individuals were successfully mated compared to >90% in F1 hybrids) and reduced fertility (49% reduction in seed set compared to F1 hybrids) (Walter et al. 2016). Consequently, we divided the F2 individuals that produced flowers into three replicate crossing lines to maintain replicates of the construction of the ARF. We then randomly mated among all F2 individuals within each line (n = 4-12 families/F2 cross type; total F2 families crossed N = 202) to produce the F3 generation (N = 259 families), ensuring that each family contributed equally. We then produced the F4 generation by first growing one individual from each F3 family and randomly designating each individual as a sire or dam. We then mated 115 sires to 114 dams in a full-sibling, half-sibling crossing design to produce 198 families for the F4 generation. The numbers of families and individuals used to create each generation of the ARF are listed in Table S1.

In the following analyses we examine results from two experiments using the ARF. In experiment 1, we grew the ARF in the glasshouse to estimate genetic variance underlying morphological traits. In experiment 2, we transplanted seeds of the ARF into the four habitats to compare the fitness of the ARF with the parental ecotypes. We then used the field fitness of the ARF (experiment 2) to quantify the genetic covariance in performance among transplant habitats and identify genotype-by-environment interactions that would indicate genetic trade-offs among habitats. Finally, to quantify differences in natural selection among habitats, we combined the data from both experiments and estimated the genetic covariance between morphological traits in the glasshouse (experiment 1) and field fitness in each habitat (experiment 2).

Experiment 1: Glasshouse phenotypes

To estimate genetic variance underlying morphological traits we grew four individuals from each full sibling family of the ARF (n = 198 full-sibling families, total N = 770 individuals) in 30 cell growth trays containing the same potting media described above. Alongside the ARF we grew four individuals from ~25 full sibling families for each of the parental ecotypes (N = 366 individuals). Plants were grown in a 25°C controlled temperature room with a 12h:12h day:night photoperiod. After eight weeks of growth we measured plant height and sampled one fully mature leaf for each plant. We used the software 'Lamina' to analyse the scanned leaf and quantify six variables relating to leaf size and leaf shape (Bylesjo et al. 2008). Using the outputs of Lamina, we quantified leaf morphology using leaf area, leaf area^2 / leaf perimeter^2 as a measure of leaf complexity, leaf circularity, number of indents standardized by leaf perimeter, leaf indent width and leaf indent depth.

Experiment 2: Field transplant

Seeds from the F4 generation of the ARF were transplanted into each of the habitats. At each transplant habitat, we planted 18 seeds from each full-sibling family (n = 198) divided equally amongst six experimental blocks (habitat $n \approx$ 3,500 seeds, total N = 14,265 seeds). Alongside the ARF we transplanted seeds from the populations of parental ecotypes used to create the ARF (for each population n = 180 seeds/habitat) (analysed previously in Walter et al. 2016). See Walter et al. (2016); Walter et al.

(2018b) for a detailed description of the field experiment. Briefly, we glued each seed to a toothpick using non-drip glue and planted them in 25mm x 25mm plastic grids in March 2014. Field observations suggested that seeds in the natural populations can germinate year-round given sufficient rain. Given we wanted to standardise germination time to estimate post-germination development and survival, to replicate natural germination conditions we suspended shadecloth (50%) 15cm above each experimental block and watered them daily for three weeks. During the initial three-week period we measured emergence and mortality daily. Following the initial three weeks we measured survival and development at weeks 4, 5, 7 and 9, and then monthly until 20 months at which time there were fewer than 20% of germinated plants remained, and we ceased the experiment. The measures of fitness we recorded were: whether each seedling emerged, whether each seedling reached 10 leaves (as a measure of seedling establishment) and produced a bud (reached maturity). All measures of fitness were collected as binary data.

Implementation of Bayesian models

In the subsequent analyses we implemented Bayesian models to 1) compare field performance (experiment 2) of the ARF with the parental ecotypes, 2) identify whether genotype-by-environment interactions create genetic trade-offs among transplant habitats (experiment 2), 3) estimate genetic (co)variance of morphological traits for the ARF (experiment 1), and 4) estimate the genetic covariance between morphological traits (experiment 1) and field performance (experiment 2), to identify differences in natural selection on morphological traits, among habitats.

All Bayesian models were implemented using R (R Core Team 2016) within the package 'MCMCglmm' (Hadfield 2010). From each model we extracted 1,000 Markov chain Monte Carlo (MCMC) samples, which provided the posterior distribution for the parameters we were estimating. For each analysis, we implemented Markov chains of different lengths (listed in Table S2), while ensuring that we included a sufficient burn-in period and thinning interval to sample the parameters with autocorrelation values of less than 0.05 and effective sample sizes exceeding 85% of the total number of samples, for all parameters. We used uninformative parameter expanded priors and checked their sensitivity by re-

implementing all models while adjusting the parameters and ensuring the posterior distribution did not change.

For the analyses estimating genetic variance, comparing estimates of genetic variance with zero provides an uninformative test of significance because estimates are restricted to be greater than zero (positive-definite). To create an informative significance test, we re-implemented each model with randomized data, created by shuffling the parental information. For each model implemented on the observed data, we re-implemented the same model on 1,000 randomizations of the data, and extracted the posterior mean for each randomization. We then compared the distribution of means from models conducted on the randomizations, to the mean of the observed posterior distribution. If the mean of the observed distribution occurred outside the 95% Highest Posterior Density (HPD) interval for the random distribution, we took this as evidence that we captured biologically important information for the comparison of interest. As we were only interested in estimating the posterior mean of models implemented on each randomization of the data, we could reduce computing time by reducing the total number of sampling iterations. To do so, we maintained the same burn-in period and sampling interval to ensure an identical mixing of MCMC chains, reducing only the total number of sampling iterations to the number required to obtain a stable estimate of the mean. We calculated the number of sampling iterations required using the models implemented on the observed data, which was different for each of the analyses outlined below (Table S2).

Comparing ARF and ecotype morphology

To compare differences in multivariate phenotype between the ARF and parental ecotypes, we implemented a multivariate analysis of variance (MANOVA) on the seven morphological traits measured in experiment 1. We first standardized all seven morphological traits to a mean of zero, and standard deviation of one before including them as a multivariate response variable. To test whether the ARF was phenotypically different to each ecotype we conducted a separate MANOVA for each pairwise comparison between the parental ecotypes, and the ARF. We used a bonferroni corrected α-value of 0.0125 ($\alpha = 0.05 / n$, where n represents the number of tests). To visualize differences among all ecotypes

and the ARF we estimate **D**, the variance-covariance matrix representing multivariate phenotypic divergence. To do so, we first conducted another MANOVA that included all ecotypes (but not the ARF). From this, we extracted the sums of squares and cross-product matrices for the ecotypes ($SSCP_H$) and error terms ($SSCP_E$) to calculate their mean-square matrices by dividing by the appropriate degrees of freedom ($MS_H = SSCP_H / 3$; $MSE = SSCP_E / 365$). Using the mean-square matrices we calculated **D** = $(MS_H - MS_E) / nf$, where *nf* represents the number of measured individuals per genotype in an unbalanced design, calculated using equation 9 in Martin et al. (2008). Our D-matrix then represents divergence in multivariate mean phenotype, among the parental ecotypes, after removing the residual phenotypic variation. To visualize the phenotypic space occupied by the ARF relative to the parental ecotypes, we decomposed **D** into orthogonal axes (eigenvectors) and calculated the phenotype scores for the first two eigenvectors for all ecotypes, and the ARF.

Comparing ARF and ecotype field performance

We estimated fitness at early life history stages for the ARF and parental ecotypes transplanted into all four habitats. To do so, we created a dummy variable that represented the ARF and native versus foreign ecotypes in each habitat. We then used MCMCglmm to implement the model,

$$\boldsymbol{y}_{ijklm} = \boldsymbol{H}_i + \boldsymbol{P}_j + \boldsymbol{H}_i \times \boldsymbol{P}_j + \boldsymbol{B}_{k(i)} + \boldsymbol{L}_{l(j)} + \boldsymbol{e}_{m(ijkl)}\,, \qquad (1)$$

where transplant habitat ($\boldsymbol{H}_i$), ARF/ecotype ($\boldsymbol{P}_j$) and their interaction ($\boldsymbol{H}_i \times \boldsymbol{P}_j$) were included as fixed effects. Blocks within transplant habitat ($\boldsymbol{B}_{k(i)}$) and replicate genetic lines within the ARF ($\boldsymbol{L}_{l(j)}$) were included as random effects, and $\boldsymbol{e}_{m(ijkl)}$ represented the model error. We implemented equation 1 with emergence, seedling establishment and maturity as a multivariate response variable ($\boldsymbol{y}_{ijklm}$). As such, for all ecotypes and the ARF, equation 1 calculated the probability of reaching maturity, conditional on the previous life history stages.

Quantifying divergent natural selection

We used the ARF to investigate differences in natural selection among contrasting natural habitats. To do so, we conducted two further analyses. First, to identify whether natural selection created genetic trade-

offs among habitats, indicated by a negative genetic covariance among habitats, we analysed field performance using a genotype-by-environment covariance framework described below. Next, we examined whether genetic selection on traits occurred in the direction of the native ecotypes. To do so, we combined the morphology data from experiment 1, with field performance data in experiment 2 and used the Robertson-Price Identity to estimate the genetic covariance between morphological traits and field performance for each transplant habitat. We predicted that if natural selection on morphology occurred in the direction of the original ecotypes, differences in selection gradients (among habitats) would align with divergence in phenotype mean of the parental ecotypes.

Genetic trade-offs among contrasting habitats

We investigated genotype-by-environment (G×E) interactions in the ARF using a character state approach, where different environments represent different traits (Robinson and Beckerman 2013). To do so, we used the field performance of the ARF and implemented

$$\boldsymbol{y}_{ijklmn} = \boldsymbol{L}_i + \boldsymbol{H}_j + \boldsymbol{S}_{k(il)} + \boldsymbol{D}_{l(ik)} + \boldsymbol{B}_{m(j)} + \boldsymbol{e}_{n(ijklm)}\,, \qquad (2)$$

where replicate genetic line of the ARF ($\boldsymbol{L}_i$) and transplant habitat ($\boldsymbol{H}_j$) were included as fixed effects. We included sire ($\boldsymbol{S}_{k(il)}$), dam ($\boldsymbol{D}_{l(ik)}$) and block within habitat ($\boldsymbol{B}_{m(j)}$) as random effects, with $\boldsymbol{e}_{n(ijklm)}$ representing the residual error variance. For each term in the random component, we estimated random intercepts for each habitat and the covariance among habitats. As such, for the sire and dam components we estimated a 4×4 covariance matrix representing variance in each habitat, and covariance among habitats. Information for estimating covariance among habitats is taken from individuals of the same full-sibling families transplanted in each habitat. Consequently, we implemented equation 2 with a heterogeneous residual covariance matrix. This allowed for different variances in each habitat, but fixed residual covariances at zero because individuals (seeds) could not be planted in two habitats simultaneously. We used three separate implementations of equation 2 for emergence, seedling establishment and maturity included as binary univariate response variables ($\mathbf{y}_{ijklmn}$).

From equation 2, $\mathbf{S}_{l(im)}$ represents one quarter of the additive genetic variance in each habitat, and one quarter of the additive genetic covariance between habitats. We multiplied the sire variance component ($\mathbf{S}_{l(im)}$) by four and used the posterior mean as our observed estimate of additive genetic (co)variance for field performance among the four habitats. The diagonal of the resulting G-matrices represents additive genetic variance within a transplant habitat, with the off diagonal representing the genetic covariance between habitats.

Divergent natural selection on morphological traits

By linking genetic variance underlying morphological traits in the laboratory, with genetic variance underlying field performance, we sought to quantify differences in natural selection among the transplant habitats using the Robertson-Price Identity. A requirement for natural selection is genetic variance in both morphological traits and field performance. The analysis of genetic variance underlying field performance (described in the previous section) identified significant genetic variance for the ability to reach maturity, in all four transplant habitats (see results). To identify the morphological traits with genetic variation we used the morphology data from experiment 1 and implemented

$$\boldsymbol{y}_{ijklmn} = \boldsymbol{L}_i + \boldsymbol{S}_{j(ik)} + \boldsymbol{D}_{k(ij)} + \boldsymbol{S}_{j(ik)} \times \boldsymbol{D}_{k(ij)} + \boldsymbol{e}_{n(ijk)}\,, \qquad (3)$$

where replicate genetic line of the ARF ($\boldsymbol{L}_i$) was included as a fixed effect and sire ($\boldsymbol{S}_{j(ik)}$), dam ($\boldsymbol{D}_{k(ij)}$) and their interaction ($\boldsymbol{S}_{j(ik)} \times \boldsymbol{D}_{k(ij)}$) were random effects, with $\boldsymbol{e}_{n(ijk)}$ as the residual variance. We implemented equation 3 with plant height and six leaf morphology traits as a multivariate response variable ($\mathbf{y}_{ijkl}$). To prevent traits on different scales affecting the analysis, we centered all traits to a mean of zero and standardized to a standard deviation of one prior to analysis. We then calculated the additive genetic (co)variance matrix as four times the sire variance component. As traits were standardized prior to analysis, genetic variances represent heritabilities. We found only four traits with heritabilities greater than 0.1 (plant height, leaf area, leaf perimeter^2 / area^2 and leaf indent width; see Table S3), which we then combined with field performance to study natural selection in the subsequent analyses, described below.

294 We estimated the genetic covariance between the morphological traits and field performance by
295 implementing the Robertson-Price Identity

296 $$R = s_g = cov(w, z)\,, \qquad (4)$$

297 where the response to selection (R) is analogous to the selection differential (s_g), calculated as the genetic
298 covariance between a trait (z) and fitness (w). Equation 4 then generalizes to multivariate form by
299 including more phenotypic traits and estimating a genetic variance-covariance matrix (**G**), with fitness as
300 the final trait. In this framework, s_g generalizes to the vector of selection gradients ($\boldsymbol{s}_g$) representing the
301 multivariate response to selection. Estimating the response to selection in this way includes both direct
302 and indirect selection. To isolate the effect of direct selection on phenotypic responses, we can calculate
303 the genetic selection gradient by combining **G** and $\boldsymbol{s}_g$ with

304 $$\boldsymbol{\beta}_g = \boldsymbol{G}^{-1}\boldsymbol{s}_g\,, \qquad (5)$$

305 where $\boldsymbol{\beta}_g$ now represents a vector of genetic selection gradients (Lande and Arnold 1983; Rausher 1992),
306 after removing the effect of genetic correlations among traits.

307 To estimate the predicted response to selection ($\boldsymbol{s}_g$) in the ARF we estimated the (co)variance between the
308 four morphology traits and field performance by implementing

309 $$\boldsymbol{y}_{ijklm} = \boldsymbol{L}_i + \boldsymbol{S}_{j(ik)} + \boldsymbol{D}_{k(ij)} + \boldsymbol{S}_{j(ik)} \times \boldsymbol{D}_{k(ij)} + \boldsymbol{B}_l + \boldsymbol{e}_{m(ijkl)}\,, \qquad (6)$$

310 where replicate genetic line ($\boldsymbol{L}_i$) was the only fixed effect. Sire ($\boldsymbol{S}_{j(ik)}$), dam ($\boldsymbol{D}_{k(ij)}$) and their interaction
311 ($\boldsymbol{S}_{j(ik)} \times \boldsymbol{D}_{k(ij)}$) were included as random effects along with block within habitat ($\boldsymbol{B}_l$). The multivariate
312 response variable ($\boldsymbol{y}_{ijklm}$) included four phenotypic traits as well as ability to reach maturity in each
313 habitat. Fitness and morphology was measured on separate individuals (field versus glasshouse
314 experiments), and so similar to equation 2, we estimated a heterogeneous residual covariance matrix.

315 Multiplying the sire variance component ($\boldsymbol{S}_{j(ik)}$) by four (from equation 6) gave the additive genetic
316 variance-covariance matrix (**G**). Elements in the first four rows and columns represented **G** among
317 morphological traits. Covariance elements in the fifth column (and row) denote the genetic covariance

between each trait and fitness (s_g), with genetic variance in fitness in the final element (fifth row, fifth column); see Stinchcombe et al. (2014) for details. We used four separate implementations of equation 6 for field performance as the ability to reach maturity in each of the four transplant habitats. We calculated the additive genetic (co)variance matrix as four times the sire variance component and extracted $\boldsymbol{s_g}$ as the vector of covariances between morphological traits and field performance (rows one to four of the fifth column).

To identify whether we captured biologically meaningful differences in selection among habitats, we conducted two analyses. First, $\boldsymbol{s}_g$ and $\boldsymbol{\beta}_g$ being vectors, we calculated the dot product (representing vector length) of the observed and random matrices. If the observed length was greater than the length calculated from the random distribution, we took this as evidence we detected biologically meaningful estimates of selection for a given habitat (Stinchcombe et al. 2014; Walsh and Lynch 2018). Second, to quantify the differences in $\boldsymbol{s}_g$ among the four transplant habitats we estimated variance is selection gradients using

$$\mathbf{Z} = \begin{pmatrix} \boldsymbol{\sigma}^2(\boldsymbol{s}_{g1}) & \boldsymbol{\sigma}(\boldsymbol{s}_{g1}, \boldsymbol{s}_{g2}) & \dots & \boldsymbol{\sigma}(\boldsymbol{s}_{g1}, \boldsymbol{s}_{gn}) \\ & \boldsymbol{\sigma}^2(\boldsymbol{s}_{g2}) & \ddots & \vdots \\ & & & \boldsymbol{\sigma}^2(\boldsymbol{s}_{gn}) \end{pmatrix}, \qquad (7)$$

where **Z** then represents the among-habitat variance in $\boldsymbol{s}_{\mathbf{g}}$ for the *n*th trait along the diagonal. The off-diagonal then contains the covariance in $\boldsymbol{s}_g$ among habitats, for each bivariate trait combination (Chenoweth et al. 2010). In the same way, we used equation 7 to calculate **B**, the among-habitat (co)variance in $\boldsymbol{\beta}_g$. Comparing the eigenvalues of observed and random (for both **B** and **Z**) provided tests of significance. Observed eigenvalues with values greater than the random distribution of eigenvalues suggested we captured greater among-habitat differences in selection than expected by random sampling.

Results

Comparing ARF and ecotype morphology

Ecotypes showed strong differences in leaf morphology (Figure 1A), with the ARF exhibiting large variation, intermediate to the parental ecotypes (Figure 1B). Pairwise MANOVAs showed the ARF was significantly different to all ecotypes (Dune: Wilks' $\lambda = 0.71$, $F_{1,857} = 50.782$, $P = <0.001$; Headland:

342 Wilks' $\lambda = 0.64$, $F_{1,863} = 69.747$, $P = <0.001$; Tableland: Wilks' $\lambda = 0.38$, $F_{1,866} = 192.36$, $P = <0.001$;
343 Woodland: Wilks' $\lambda = 0.22$, $F_{1,864} = 445.1$, $P = <0.001$). The MANOVA conducted on only the parental
344 ecotypes described a significant difference among ecotypes in multivariate mean phenotype (Wilks' $\lambda =$
345 0.03, $F_{3,362} = 117.86$, $P = <0.001$), where differences among ecotypes captured 64% of the total variance.
346 The first eigenvector of **D** ($\boldsymbol{d}_{max}$) described 84% of phenotypic divergence mostly created by phenotypic
347 differences between the Tableland and Headland ecotypes (Figure 1D). The second eigenvector ($\boldsymbol{d}_2$)
348 described 14% of variation in multivariate phenotype, describing differences between the Woodland and
349 Tableland ecotypes (Figure 1D). The ARF occupied an area in phenotypic space close to the Dune
350 ecotype, and intermediate between the Headland, Tableland and Woodland ecotypes. However, the ARF
351 mean was not similar to that of the overall mean of all ecotypes, but exhibited high phenotypic variance
352 that appeared to be missing some of the extreme phenotypes, especially from the Tableland and
353 Woodland ecotypes (Figure 1D).

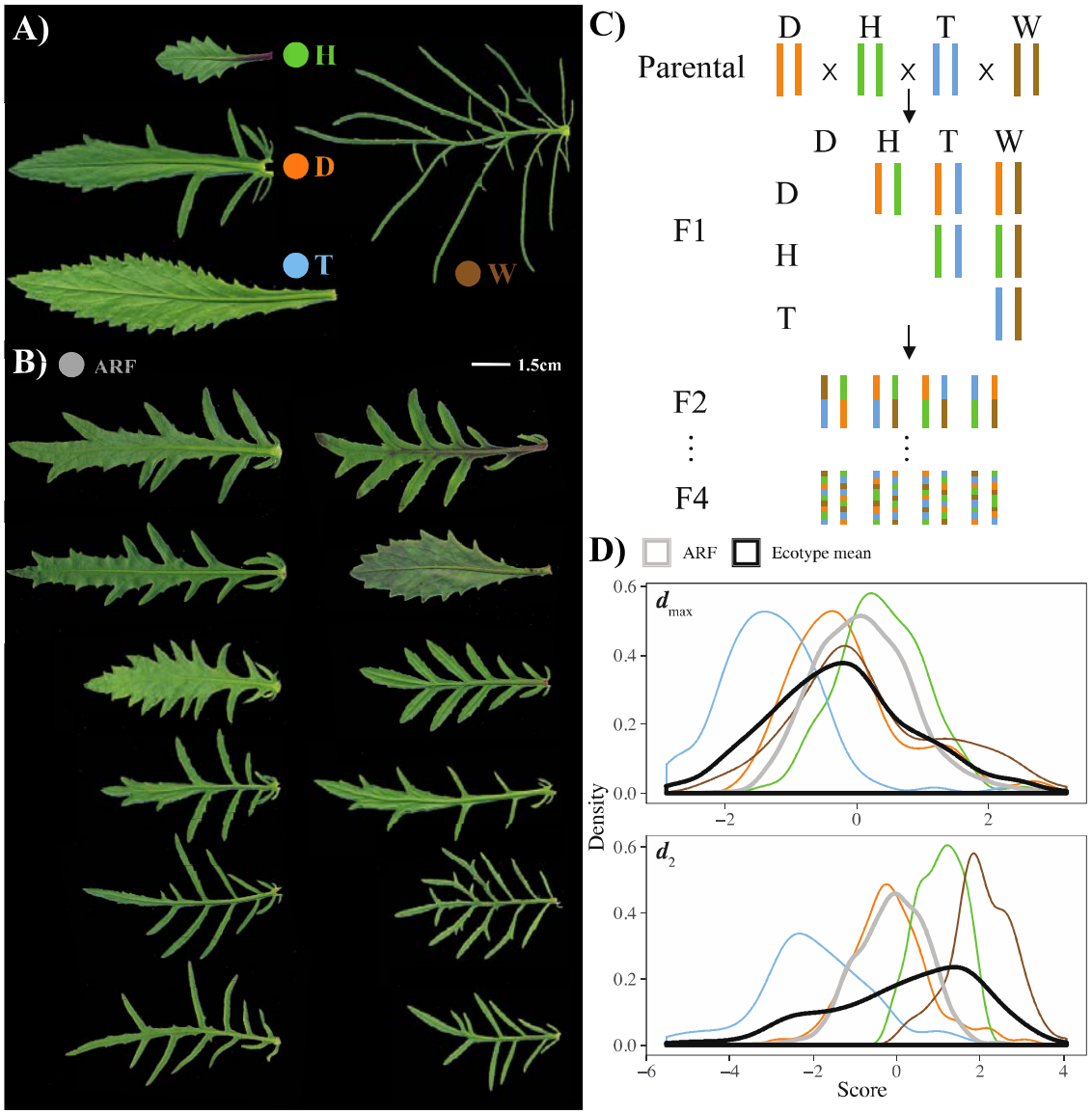

Figure 1: A) Ecotypes vary dramatically in leaf morphology. **B)** The ARF exhibited large variation in leaf morphology, visually intermediate among the original ecotypes. **C)** The ARF was created by equally mating among all ecotypes. **D)** The distribution of ecotype and ARF scores for the first two axes of **D** showing the ARF (grey) occupying an area in phenotypic space similar to the mean of all ecotypes (black), but lacking extreme phenotypes, especially of the Tableland and Woodland ecotypes.

Comparing ARF and ecotype field performance

Given ecotypes have shown adaptation to their contrasting habitats (Walter et al. 2016; Walter et al. 2018b), we expected that as an intermediate form, the ARF would show intermediate performance between native and foreign populations. We found the performance of the ARF was similar to the native ecotypes for seedling establishment and maturity (Figure 2), suggesting hybrid vigor despite several generations of recombination.

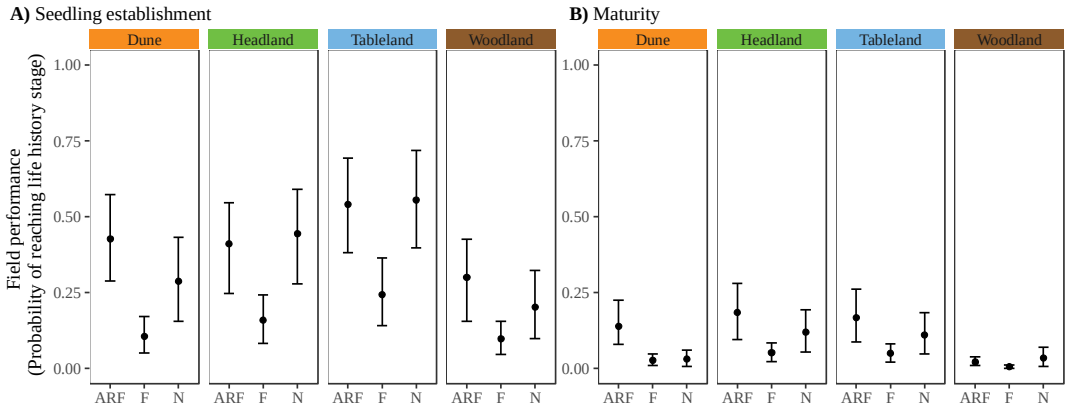

Figure 2: Field performance of the ARF compared to foreign (F) and native (N) ecotypes in each transplant habitat. Fitness measured as the probability of reaching **A)** seedling establishment, and **B)** maturity. Credible intervals represent 95% HPD intervals.

Genetic trade-offs among contrasting habitats

If habitat-specific natural selection creates genetic trade-offs between contrasting habitats, we expected the ARF to show genetic variance for field fitness, and negative genetic covariance between contrasting habitats. However, given the ARF lacked the extreme phenotypes of the Headland, Tableland and Woodland ecotypes (Figure 1), and exhibited relatively high field performance (Figure 2), we might expect low genetic variance associated with either zero genetic covariance or a positive genetic covariance between habitats. We found that across the four habitats, additive genetic variance increased as life history stages progressed (Figure 3). Observed estimates of genetic variance in field performance were within the random distribution at emergence, but were greater than the random distribution for maturity (Figure 3). In the headland and tableland habitats we detected lower genetic variance than expected by chance for seedling establishment.

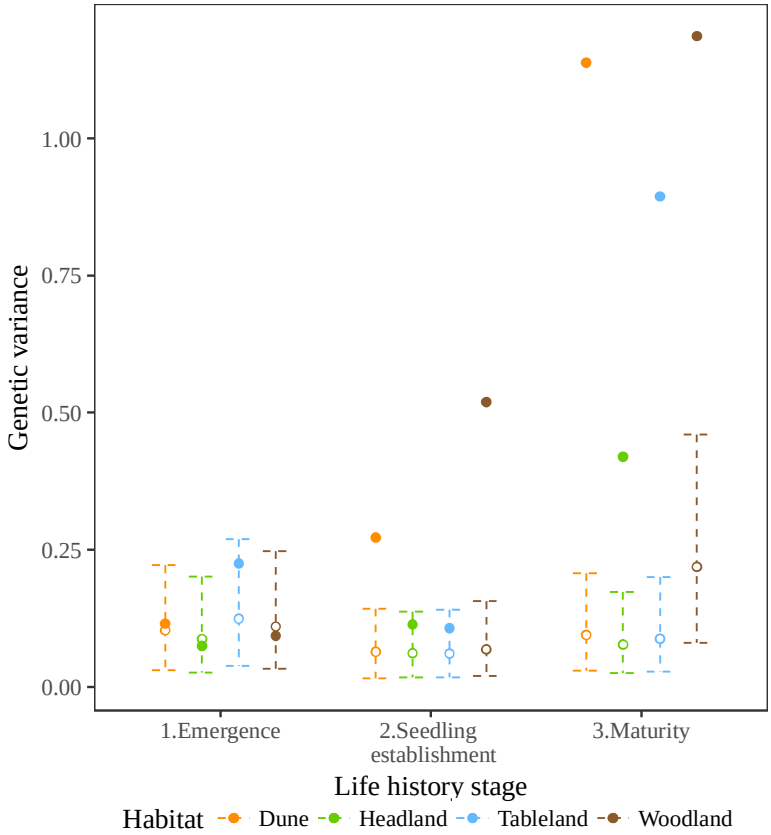

Figure 3: Genetic variance for field performance in the ARF for each habitat (coloured circles and lines) and at each life history stage. Filled circles represent the observed estimates of genetic variance, with dashed lines and unfilled circles representing the random distribution. Additive genetic variance in fitness increased through life history. Credible intervals represent 95% HPD intervals.

Decomposing the genetic covariance matrix described orthogonal axes of genetic variation underlying field fitness. Decomposing the matrix for each life history stage, we found the first three eigenvectors for maturity described more genetic variance than expected under random sampling (Figure 4). Interpreting the loadings of each eigenvector reveal how each habitat contributes to describing the genetic variance in fitness quantified by that eigenvector. Habitats with loadings of the same sign describe shared genetic variance for fitness, whereas loadings of different signs describe differences in genetic variance and provide evidence of fitness trade-offs. We found all habitats contributed equally to describing genetic variance underlying the first eigenvector, suggesting it described heterosis or shared genetic variation needed to function in stressful environments (Table 1). However, eigenvectors two and three provided evidence of genetic tradeoffs, describing genetic variance in fitness that differed between the woodland and dune ecotypes ($\boldsymbol{e}_2$), and between the tableland, and the dune and woodland transplant habitats ($\boldsymbol{e}_3$; Table 1). Eigenvector 4 did not describe biologically meaningful genetic variance (Figure 4), but described differences in genetic variance between the headland, and dune and tableland habitats. The

399 posterior mean G-matrices and genetic correlations for field performance are located in supplementary
400 Table S4.

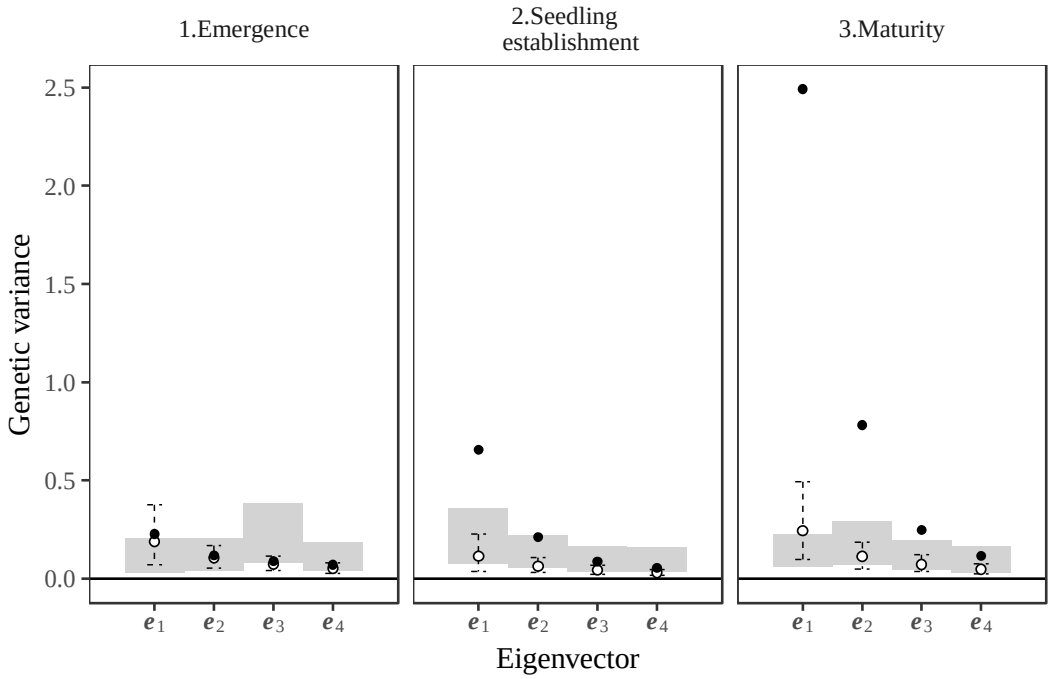

401
402 **Figure 4:** Comparing the amount of genetic variance described by eigenvectors representing the observed (filled circles)
403 versus random matrices (unfilled circles and dashed lines), for each life history stage. Gray bars represent the amount of
404 genetic variance in the randomized matrices described by the observed eigenvectors. Only the first three eigenvectors for
405 maturity described more genetic variance than expected by random sampling. Credible intervals represent 95% HPD intervals.

406 **Table 1:** Eigenanalysis of the additive genetic (co)variance matrix for field performance at maturity. Loadings in bold are
407 greater than 0.25 to aid interpretation. HPD represents the observed 95% HPD credible intervals.

	Eigenvectors	e_1	e_2	e_3	e_4
	Eigenvalue	2.492	0.782	0.248	0.116
	HPD	0.837-4.179	0.036-1.984	0.037-0.569	0.011-0.267
	Proportion	0.685	0.215	0.068	0.032
Habitat	Dune	**-0.56**	**0.61**	**0.45**	**-0.34**
	Headland	**-0.34**	0.22	-0.04	**0.91**
	Tableland	**-0.54**	-0.02	**-0.81**	**-0.23**
	Woodland	**-0.53**	**-0.76**	**0.37**	0.00

408
409 Overall, our results showed strong patterns of adaptive divergence (Figure 2), and although there appears
410 to be a common genetic basis to fitness in all environments ($\boldsymbol{e}_1$; Table 1) we also detected genetic trade-
411 offs for fitness among certain habitats (Table 1). Despite strong adaptive divergence in Figure 2, the
412 headland and tableland habitats exhibited weaker additive genetic variance for fitness (Figure 5), and
413 weaker genetic trade-offs with other environments (Table 1), when compared to the dune and woodland.
414 This suggested alleles lost during F2 hybrid breakdown contributed to both genetic incompatibilities and

adaptive genetic variation that was lost in the ARF, reducing genetic variance for field performance in certain environments and producing weaker genetic trade-offs than expected. To test this, for each habitat we compared the strength of adaptive divergence (Figure 2; native ecotype performance – foreign ecotype performance) against the level of genetic variance exhibited by the ARF. As predicted, we found a strong negative association for seedling establishment and a weaker negative association for maturity (Figure 5), suggesting alleles associated with strong adaptive divergence were also responsible for genetic incompatibilities.

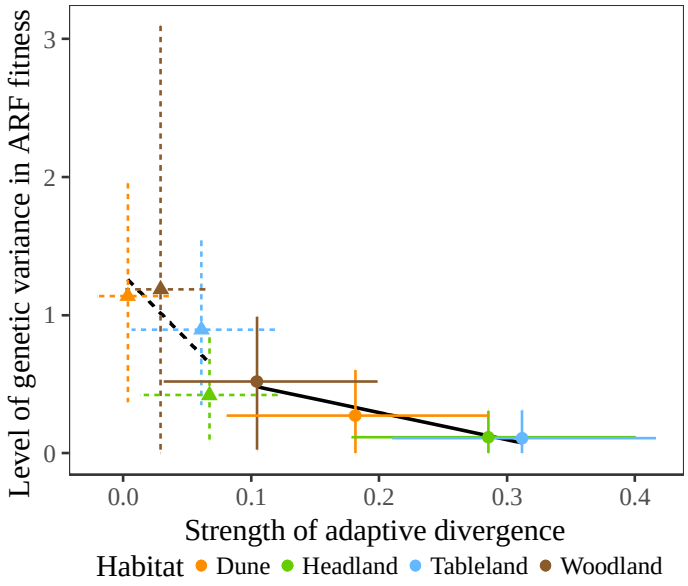

Figure 5: Stronger adaptive divergence was negatively associated with the level of genetic variance. The strength of adaptive divergence measured as the difference in fitness between the native ecotype and foreign parental ecotypes, versus the level of genetic variance in the ARF, for the same habitat. Solid circles and lines represent seedling establishment, triangles and dashed lines represent the ability to reach maturity. Credible intervals represent 95% HPD intervals. Estimating a regression slope for each MCMC iteration showed a significant negative association at 88% HPD for seedling establishment, but a non-significant relationship for maturity.

Natural selection on morphological traits

To quantify selection in each habitat we calculated $\boldsymbol{s}_g$ as the genetic covariance between morphological traits measured in the glasshouse, and field performance measured in each of the four transplant habitats. We then isolated direct selection by calculating $\boldsymbol{\beta}_g$, the genetic selection gradient for each habitat. Comparing the length of observed and random $\boldsymbol{s}_g$ and $\boldsymbol{\beta}_g$ suggested we captured biologically meaningful selection within each habitat (Figure S5A). To quantify differences in selection among habitats we estimated **B** and **Z** as the among-habitat (co)variance in selection vectors. Comparison of observed and random eigenvalues showed that both selection vectors exhibited greater differences among habitats than

expected by random sampling (Figure S5B), suggesting differences in our observed selection vectors described biologically meaningful differences in natural selection among transplant habitats.

If differences in natural selection among the four habitats occurred in the direction of adaptive evolution, we would expect differences in $\boldsymbol{s}_g$, but not $\boldsymbol{\beta}_g$, to align with divergence in mean phenotype of the parental ecotypes. Eigenanalyis of **B** and **Z** quantifies the axes that describe differences among the original selection vectors, with the first axis for each matrix representing 83% (HPD 56-98%) and 81% (HPD 55-98%) of the total variance, respectively. We tested whether the first axis from each selection vector aligned with $\boldsymbol{d}_{max}$, the axis describing the greatest difference in multivariate phenotype mean. To do so, we calculated the angle between the first eigenvector of **B** and **Z**, and $\boldsymbol{d}_{max}$. We found the alignment between **Z** and **D**, but not **B,** was closer than expected with random sampling (Figure 6A). To complement this analysis, we conducted a more extensive analysis using a covariance tensor approach, which is provided in supplementary material. Results obtained from both analyses matched closely, suggesting the response to selection, but not the direction of selection, aligned with divergence in parental ecotype morphology.

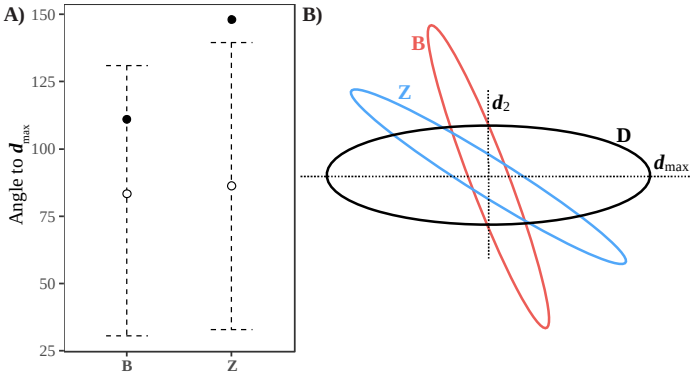

Figure 6: Differences in $\boldsymbol{s}_g$, but not $\boldsymbol{\beta}_g$, aligned with $\boldsymbol{d}_{max}$, but differences in $\boldsymbol{\beta}_g$ aligned with $\boldsymbol{d}_2$. **A)** The angle between the first eigenvector of **Z**, and $\boldsymbol{d}_{max}$ was closer than expected by random sampling, but the first eigenvector of **B** did not show a close alignment with $\boldsymbol{d}_{max}$. Credible intervals represent 90% HPD intervals. **B)** Two-dimensional schematic approximately representing the orientation of **B** and **Z** in relation to **D**, and $\boldsymbol{d}_{max}$.

Discussion

Here, we have used ecotype-specific genetic variation to connect adaptation and speciation during adaptive radiation. We found that an ARF exhibited a multivariate phenotype intermediate to the four parental ecotypes, but was lacking in much of the phenotypic variation of the parental ecotypes. Genetic variance for fitness in the ARF was lower when transplanted into habitats associated with stronger

differences between native and foreign parental fitness. Genetic trade-offs in field performance among habitats were only observed in axes describing smaller amounts of genetic variance underlying field fitness. Despite only one generation of selection, among-habitat differences in the response to selection aligned with the direction of morphological divergence of the original ecotypes, but only when genetic correlations were removed. Together, our results provide empirical evidence suggesting interactions between genetic incompatibilities and divergent natural selection created adaptive radiation of an Australian wildflower into four contrasting habitats.

While there is abundant evidence implicating divergent natural selection in the accumulation of extrinsic reproductive barriers such as immigrant inviability and ecologically dependent postzygotic isolation (reviewed in Baack et al. 2015), the contribution of adaptation to the evolution of genetic incompatibilities during population divergence remains unresolved (Baack et al. 2015). Many genes underlying postzygotic isolation show the signature of past rapid evolution, but connecting genes underlying both adaptation and reproductive isolation are rare (Presgraves 2010). In *Mimulus guttatus*, a gene underlying copper tolerance was also associated with genetic incompatibilities (Macnair and Christie 1983). Our results further clarify the connection between adaptation and the evolution of genetic incompatibilities by showing that intrinsic reproductive isolation in F2 hybrids was associated with the loss of extreme phenotypic variation, and the alleles underlying these incompatibilities were likely adaptive.

We suggest that environment-specific dominant alleles link extreme phenotypes with natural selection and reproductive isolation to create adaptive radiation in these contrasting ecotypes. This is because heterozygotes (with alleles from different ecotypes) at one or more loci underlie F2 hybrid breakdown, creating negative additive × dominant or dominant × dominant interactions (Demuth and Wade 2005; Willett 2006), suggesting genetic incompatibilities at the F2 generation are largely produced by dominant alleles (e.g., Sweigart et al. 2006; Latta et al. 2007). Our F2 hybrid was constructed by mating between two completely unrelated F1 crosses (Figure 1C; e.g., $F1_{Dune,Headland} \times F1_{Tableland,Woodland}$), increasing heterozgosity compared to traditional F2 crosses between two populations, and reducing the likelihood of

homozygous recessive loci (detailed explanation of the crossing design is located in supplementary material). Dominant alleles will be more visible to selection, allowing them to increasing in frequency rapidly and create rapid adaptive divergence. Whether these alleles then contribute to the evolution of stronger genetic incompatibilities (e.g., F1 hybrid breakdown) remains unexplored.

F2 hybrid breakdown indicates population divergence as a build-up of coadapted gene complexes, created when selection assembles beneficial combinations of alleles (Cutter 2012; Corbett-Detig et al. 2013). In this system, it is likely the evolution of coadapted gene complexes were responsible for the rise of intrinsic reproductive isolation during the early stages of speciation (Corbett-Detig et al. 2013). We can then view the evolution of these ecotypes from a perspective where selection acts upon additive genetic variation by increasing allele frequencies at independent loci (Hill et al. 2008), but limited recombination due to small population size, maladaptive gene flow or strong selection creates coadapted gene complexes (Mayr 1954; Carson and Templeton 1984; Ortiz-Barrientos et al. 2016). The strength of coadaptation within a population will then determine how genetic incompatibilities arise among populations and lead to speciation.

The strength of divergence (and consequently, reproductive isolation) among coadapted gene complexes will be population and environment specific, and depend on the interaction between mutation, migration, drift and selection. Previous studies of Dune-Headland parapatric pairs along the Australian coastline have shown convergent evolution, suggesting multiple independent origins of these ecotypes (Roda et al. 2013b; Roda et al. 2017). If the same dominant alleles important for adaptation to these contrasting environments are repeatedly selected in the same environment, they may form coadapted gene complexes within populations of each environment, with drift or local adaptation causing differences among localities (Goodnight 2000). Whether locally adapted coadapted gene complexes between locations of the same species will give rise to reproductive isolation remains unexplored, but could provide important insights into the relationship between adaptation and divergence across a heterogeneous landscape.

Genetic variance for life history and fitness traits is often low (e.g., McFarlane et al. 2014), and often decreases with ontogeny (e.g., Aguirre et al. 2014). In contrast, we showed increased genetic variance

513 with development, results similar to recent studies in the laboratory (Styga et al. 2018). Changes in
514 genetic variance underlying fitness have profound implications for understanding adaptation and
515 responses to environmental change (Sgrò and Hoffmann 2004). If genetic correlations among traits under
516 selection change during ontogeny, the effects of selection will not be linear as organisms develop and will
517 depend on changes in the combination of genetic variation and selection pressures over time. As different
518 trait combinations will be available to selection at different developmental points, patterns of adaptation
519 will be determined by the combination of traits visible when selection is strong (Bourret et al. 2017; Styga
520 et al. 2018). Consequently, it will be important to consider the relationship between changes in genetic
521 correlations and changes in natural selection, as development proceeds.

522 The alignment of phenotypic divergence (**D**) with differences in the response to selection ($\boldsymbol{s}_g$), but not the
523 genetic selection gradients ($\boldsymbol{\beta}_g$), suggests that constraints to adaptation would exist if the ARF was left to
524 evolve in the natural environments. This is because after one generation of selection, the mean phenotype
525 was expected to follow divergence towards the parental ecotypes, but selection in the absence of genetic
526 correlations among traits was in a direction different to phenotypic divergence. We must be circumspect
527 in this interpretation because estimation of $\boldsymbol{\beta}_g$ assumes we have included all traits under selection,
528 whereas $\boldsymbol{s}_g$ does not suffer from the same limitation (Morrissey et al. 2012; Stinchcombe et al. 2014).
529 However, this caveat applies to predicting future natural selection, and is less important for our analyses
530 because we are testing whether genetic architecture ($\boldsymbol{s}_g$) or the directions of selection ($\boldsymbol{\beta}_g$), predicts the
531 result of past evolutionary divergence (**D**).

532 Previously we showed that genetic variance has evolved, and diverged among these ecotypes, which
533 aligned with the direction of morphological evolution (Walter et al. 2018a). This suggested that genetic
534 constraints have limited capacity to constrain adaptation during adaptive radiation, or genetic variance
535 can evolve to reduce genetic constraints as evolution proceeds. Given we observed ecotypic divergence in
536 the genetic relationship among traits (Walter et al. 2018a), but also genetic constraints in the ARF after
537 ecotype-specific adaptive alleles were lost, we believe the loss of ecotype-specific adaptive alleles has re-
538 created the constraints present during the very early stages of adaptive divergence. During the early stages

of adaptive radiation, adaptation will be constrained to follow $\boldsymbol{g}_{\max}$ (Lande and Arnold 1983; Arnold 1992; Schluter 1996). As environment specific adaptive alleles increase in frequency, $\boldsymbol{g}_{\max}$ alters to align with the phenotypic optimum and evolution is determined by the long-term correlated response to selection (Zeng 1988). Thus, adaptive radiation occurs when environment-specific alleles increase in frequency, causing changes in the distribution of genetic variance and ameliorates genetic constraints as adaptive divergence proceeds.

In conclusion, we identified patterns of phenotypic and adaptive divergence among recently derived ecotypes, created by the accumulation of environment-specific alleles in response to natural selection. We show that these alleles likely created ecotype-specific adaptive phenotypes and fitness trade-offs between habitats that also lead to genetic incompatibilities between divergent ecotypes and reduced genetic constraints to adaptation in response to divergent natural selection. Through these experiments we identify the connection between microevolutionary genetic changes and macroevolutionary diversification in the context of an adaptive radiation.

Acknowledgements

We are indebted to Mal Smith, Ruth and Andrew Shaw, and the Ballina Shire Council for generously allowing access to the transplant sites. We are very grateful to M. James, C. Palmer, S. Edgley, J. Walter, L. Ambrose, B. Ayalon, S. Carrol, M. Gallo, F. Roda, A. Maynard, and H. North for their help with the fieldwork. This project was funded by Australian Research Council grants to DO-B.

References

Aguirre, J. D., M. W. Blows, and D. J. Marshall. 2014. The genetic covariance between life cycle stages separated by metamorphosis. Proceedings of the Royal Society B-Biological Sciences 281.

Ali, S. I. 1969. *Senecio lautus* Complex in Australia .5. Taxonomic interpretations. Australian Journal of Botany 17:161-176.

Anderson, J. T., C. R. Lee, C. A. Rushworth, R. I. Colautti, and T. Mitchell-Olds. 2013. Genetic trade-offs and conditional neutrality contribute to local adaptation. Molecular Ecology 22:699-708.

Anderson, J. T., J. H. Willis, and T. Mitchell-Olds. 2011. Evolutionary genetics of plant adaptation. Trends in Genetics 27:258-266.

Arnold, S. J. 1992. Constraints on Phenotypic Evolution. The American Naturalist 140:S85-S107.

Baack, E., M. C. Melo, L. H. Rieseberg, and D. Ortiz-Barrientos. 2015. The origins of reproductive isolation in plants. New Phytologist.

Bourret, A., M. Bélisle, F. Pelletier, and D. Garant. 2017. Evolutionary potential of morphological traits across different life-history stages. Journal of Evolutionary Biology 30:616-626.

Bylesjo, M., V. Segura, R. Y. Soolanayakanahally, A. M. Rae, J. Trygg, P. Gustafsson, S. Jansson et al. 2008. LAMINA: a tool for rapid quantification of leaf size and shape parameters. BMC Plant Biology 8.

Carson, H. L., and A. R. Templeton. 1984. Genetic Revolutions in Relation to Speciation Phenomena - the Founding of New Populations. Annual Review of Ecology and Systematics 15:97-131.

Chenoweth, S. F., H. D. Rundle, and M. W. Blows. 2010. The contribution of selection and genetic constraints to phenotypic divergence. The American Naturalist 175:186-196.

Cheverud, J. M. 1982. Phenotypic, Genetic, and Environmental Morphological Integration in the Cranium. Evolution 36:499-516.

Corbett-Detig, R. B., J. Zhou, A. G. Clark, D. L. Hartl, and J. F. Ayroles. 2013. Genetic incompatibilities are widespread within species. Nature 504:135-137.

Coyne, J. A., and H. A. Orr. 2004, Speciation. Sunderland, MA, Sinauer Associates.

Cutter, A. D. 2012. The polymorphic prelude to Bateson-Dobzhansky-Muller incompatibilities. Trends in Ecology & Evolution 27:209-218.

Demuth, J. P., and M. J. Wade. 2005. On the theoretical and empirical framework for studying genetic interactions within and among species. The American Naturalist 165:524-536.

Dobzhansky, T. G. 1937, Genetics and the origin of species. New York, Columbia University Press.

Doroszuk, A., M. W. Wojewodzic, G. Gort, and J. E. Kammenga. 2008. Rapid divergence of genetic variance-covariance matrix within a natural population. The American Naturalist 171:291-304.

Eroukhmanoff, F., and E. I. Svensson. 2011. Evolution and stability of the G-matrix during the colonization of a novel environment. Journal of Evolutionary Biology 24:1363-1373.

Goodnight, C. J. 2000. Quantitative trait loci and gene interaction: the quantitative genetics of metapopulations. Heredity (Edinb) 84:587-598.

Hadfield, J. D. 2010. MCMC Methods for Multi-Response Generalized Linear Mixed Models: The MCMCglmm R Package. Journal of Statistical Software 33:1-22.

Hill, W. G., M. E. Goddard, and P. M. Visscher. 2008. Data and theory point to mainly additive genetic variance for complex traits. PLoS Genet 4:e1000008.

Kondrashov, A. S. 2003. Accumulation of Dobzhansky-Muller incompatibilities within a spatially structured population. Evolution 57:151-153.

Lande, R. 1979. Quantitative Genetic Analysis of Multivariate Evolution, Applied to Brain:Body Size Allometry. Evolution 33:402-416.

Lande, R., and S. J. Arnold. 1983. The Measurement of Selection on Correlated Characters. Evolution 37:1210-1226.

Latta, R. G., K. M. Gardner, and A. D. Johansen-Morris. 2007. Hybridization, recombination, and the genetic basis of fitness variation across environments in *Avena barbata*. Genetica 129:167-177.

Macnair, M. R., and P. Christie. 1983. Reproductive isolation as a pleiotropic effect of copper tolerance in *Mimulus guttatus?* Heredity 50:295-302.

Martin, G., E. Chapuis, and J. Goudet. 2008. Multivariate Q_{st}–F_{st} Comparisons: A Neutrality Test for the Evolution of the G Matrix in Structured Populations. Genetics 180:2135-2149.

Mayr, E. 1954. Change of genetic environment and evolution, Pages 157-180 *in* J. Huxley, A. C. Hardy, and E. B. Ford, eds. Evolution as a process. London, Allen and Unwin.

McFarlane, S. E., J. C. Gorrell, D. W. Coltman, M. M. Humphries, S. Boutin, and A. G. McAdam. 2014. Very low levels of direct additive genetic variance in fitness and fitness components in a red squirrel population. Ecology and Evolution 4:1729-1738.

Melo, M. C., A. Grealy, B. Brittain, G. M. Walter, and D. Ortiz-Barrientos. 2014. Strong extrinsic reproductive isolation between parapatric populations of an Australian groundsel. New Phytologist 203:323-334.

Morrissey, M. B., D. J. Parker, P. Korsten, J. M. Pemberton, L. E. Kruuk, and A. J. Wilson. 2012. The prediction of adaptive evolution: empirical application of the secondary theorem of selection and comparison to the breeder's equation. Evolution 66:2399-2410.

Muller, H. J. 1942. Isolating mechanisms, evolution and temperature. Biology Symposium 6.

Navarro, A., and N. H. Barton. 2003. Accumulating postzygotic isolation genes in parapatry: a new twist on chromosomal speciation. Evolution 57:447-459.

Ortiz-Barrientos, D., J. Engelstädter, and L. H. Rieseberg. 2016. Recombination Rate Evolution and the Origin of Species. Trends in Ecology & Evolution 31:226-236.

Presgraves, D. C. 2010. Darwin and the Origin of Interspecific Genetic Incompatibilities. The American Naturalist 176:S45-S60.

Pujol, B., S. Blanchet, A. Charmantier, E. Danchin, B. Facon, P. Marrot, F. Roux et al. 2018. The Missing Response to Selection in the Wild. Trends in Ecology & Evolution 33:337-346.

R Core Team. 2016.R: A language and environment for statistical computing, version v. 3.3.2.R Foundation for Statistical Computing, Vienna, Austria.

Radford, I. J., R. D. Cousens, and P. W. Michael. 2004. Morphological and genetic variation in the *Senecio pinnatifolius* complex: are variants worthy of taxonomic recognition? Australian Systematic Botany 17:29-48.

Rausher, M. D. 1992. The Measurement of Selection on Quantitative Traits: Biases Due to Environmental Covariances between Traits and Fitness. Evolution 46:616-626.

Richards, T. J., and D. Ortiz-Barrientos. 2016. Immigrant inviability produces a strong barrier to gene flow between parapatric ecotypes of *Senecio lautus*. Evolution 70:1239-1248.

Richards, T. J., G. M. Walter, K. McGuigan, and D. Ortiz-Barrientos. 2016. Divergent natural selection drives the evolution of reproductive isolation in an Australian wildflower. Evolution 70:1993-2003.

Robinson, M. R., and A. P. Beckerman. 2013. Quantifying multivariate plasticity: genetic variation in resource acquisition drives plasticity in resource allocation to components of life history. Ecology Letters 16:281-290.

Roda, F., L. Ambrose, G. M. Walter, H. L. L. Liu, A. Schaul, A. Lowe, P. B. Pelser et al. 2013a. Genomic evidence for the parallel evolution of coastal forms in the *Senecio lautus* complex. Molecular Ecology 22:2941-2952.

Roda, F., H. L. Liu, M. J. Wilkinson, G. M. Walter, M. E. James, D. M. Bernal, M. C. Melo et al. 2013b. Convergence and Divergence during the Adaptation to Similar Environments by an Australian Groundsel. Evolution 67:2515-2529.

Roda, F., G. M. Walter, R. Nipper, and D. Ortiz-Barrientos. 2017. Genomic clustering of adaptive loci during parallel evolution of an Australian wildflower. Molecular Ecology 26:3687-3699.

Schluter, D. 1996. Adaptive radiation along genetic lines of least resistance. Evolution 50:1766-1774.

Sgrò, C. M., and A. A. Hoffmann. 2004. Genetic correlations, tradeoffs and environmental variation. Heredity 93:241-248.

Stinchcombe, J. R., A. K. Simonsen, and M. W. Blows. 2014. Estimating Uncertainty in Multivariate Responses to Selection. Evolution 68:1188-1196.

Styga, J. M., T. M. Houslay, A. J. Wilson, and R. L. Earley. 2018. Development of G: a test in an amphibious fish. Heredity.

Sweigart, A. L., L. Fishman, and J. H. Willis. 2006. A simple genetic incompatibility causes hybrid male sterility in *Mimulus*. Genetics 172:2465-2479.

Walsh, B., and M. W. Blows. 2009. Abundant Genetic Variation plus Strong Selection = Multivariate Genetic Constraints: A Geometric View of Adaptation. Annual Review of Ecology Evolution and Systematics 40:41-59.

Walsh, B., and M. Lynch. 2018, Evolution and selection of quantitative traits. Oxford, Oxford University Press.

Walter, G. M., J. D. Aguirre, M. W. Blows, and D. Ortiz-Barrientos. 2018a. Evolution of genetic variance during adaptive radiation. The American Naturalist 191:E108–E128.

Walter, G. M., M. J. Wilkinson, J. D. Aguirre, M. W. Blows, and D. Ortiz-Barrientos. 2018b. Environmentally induced development costs underlie fitness tradeoffs. Ecology 99:1391–1401.

Walter, G. M., M. J. Wilkinson, M. E. James, T. J. Richards, J. D. Aguirre, and D. Ortiz-Barrientos. 2016. Diversification across a heterogeneous landscape. Evolution 70:1979-1992.

Willett, C. S. 2006. Deleterious epistatic interactions between electron transport system protein-coding loci in the copepod *Tigriopus californicus*. Genetics 173:1465-1477.

Zeng, Z. B. 1988. Long-Term Correlated Response, Interpopulation Covariation, and Interspecific Allometry. Evolution 42:363-374.